Extreme Equatorial Scintillation

Chuck Rino

November 2026

Abstract

The statistical theory of scintillation generally refers to a hierarchy of complex field moment equations functionally defined by refractive-index structure functions. The moment equations characterize strong scintillation. However, solutions are formally restricted to fields that can be represented by superpositions of plane waves subtending a narrow range of propagation angles. The multiple-phase screen (MPS) method is used extensively to generate realizations of complex scintillation. We have found that the intensity of unconstrained MPS simulations converge to speckle-like exponential probability density functions irrespective of the initiating phase screen-structure. In effect, MPS simulations extend the range of the statistical theory. We show further that phase estimates extracted from back-propagated MPS simulations retain a partially recoverable memory of initiating large-scale structure.

1 Introduction

The theory of propagation in an irregular transparent medium starts with the vector wave equation for time-harmonic fields

$$\nabla^2\mathbf{E}(\mathbf{r}) + k^2\mathbf{E}(\mathbf{r}) = -X(\mathbf{r})\overline{\chi}\mathbf{E}(\mathbf{r}) + \boldsymbol{\nabla}\left(\boldsymbol{\nabla}\cdot\mathbf{E}\right), \tag{1}$$

where $X(\mathbf{r})\overline{\chi}$ is a 3×3 complex matrix that characterizes the interaction of the field, $\mathbf{E}$, with the propagation medium. Propagation is formally defined by introducing a rectangular coordinate system with one axis serving as a propagation reference. In a uniform magnetic field $\overline{\chi}$ is constant. If the divergence term, $\boldsymbol{\nabla}\cdot\mathbf{E}$, is neglected, an eigenvector decomposition of $X(\mathbf{r})\overline{\chi}$ can be used to generate three coupled scalar equations of the form

$$\nabla^2\psi\left(x,y\right) + k^2\left(I + X\left(x,y\right)\right)\psi\left(x,y\right) = 0, \tag{2}$$

where $\psi\left(x,y\right)$ represents a component of the transformed vector wavefield. If the medium is homogeneous, solutions to (2) are superpositions of two orthogonal plane-wave characteristics modes. Generating a fully consistent solution to (1) *requires* retention of the $\boldsymbol{\nabla}\cdot\mathbf{E}$ term. Fortunately, at frequencies above HF

solving (2) with $\sqrt{1+X(x,y)}$ interpreted as a scalar refractive index characterizes the complex modulation of a circularly polarized transverse vector field component.

Even so, pursuing general solutions to (2) following scalar-field propagation methods requires computationally-demanding application-specific procedures. However, *any* solution to (2) will support a two-dimensional Fourier decomposition as a superposition of plane-wave components in the spatial domain with $\boldsymbol{\kappa}$ the transverse component of a wave propagating along the direction $\boldsymbol{k} = [\boldsymbol{\kappa}, \kappa_z]$. The propagation angle with respect to the z axis is $\theta = 2\pi\kappa/k$, where $k = 2\pi f/c$. Similarly, in the absence of diffraction ($\nabla^2\psi(x,y) \sim 0$), advancing the field a small distance forward imposes an incremental phase perturbation. This invites a split-step approximation, which introduces a phase perturbation followed by free propagation. The forward propagation equation (FPE) is effectively the differential equation form of the split-step approximation.

The FPE is strictly applicable only to fields that subtend a narrow range of propagation angles, which is the same constraint that applies to the statistical theory of scintillation and theoretical results applicable to fields initiated by a phase screen. When the free propagation of a field initiated by a phase screen generates significant structure at large propagation angles, the theory breaks down. Ramifications have been investigated by Sun et al. [1].

Extreme scintillation refers to complex fields with $S4 \geq 1$. Extreme scintillation with $S4 > 1$ is referred to as strong focusing. Structure that generates strong focusing requires only a 10 to 15 dB local enhancement as opposed to structure that can produce caustics. Furthermore, extreme scintillation with an exponentially distributed intensity and propagation angles subtending the full propagation range is not excluded from MPS simulations. Consider that the FPE and MPS increments have the same operator form

$$\psi(x+\Delta x, y) = \exp\{\widehat{D}\Delta x\}\exp\{\widehat{V}\Delta x\}, \tag{3}$$

where $\widehat{D}$ represents the diffraction operator and $\widehat{V}$ represents the phase operator. Following Fishman [2], a corrected operator form can be written as

$$\psi(x+\Delta x, y) = \exp\{\left(\widehat{D}+\widehat{V}\right)\Delta x + \frac{1}{2}\left[\widehat{D},\widehat{V}\right]\Delta x^2 + ...\} \tag{4}$$

where $\left[\widehat{D},\widehat{V}\right]$ represents a commutation operation. Strong strong gradients in $X(x,y)$ cause rapid commutation variations, whereby the commutator makes a significant contribution and cannot be neglected. Conversely, fine-scale structure in $\psi(x,y)$, which is implied by an extended range of propagation angles, causes $\widehat{D}$ to decrease the commutator contribution. It follows that MPS simulations of propagation in random media can accommodate stochastic structure over the full range of propagation angles as long as background gradients would not otherwise contribute.

2 Unconstrained MPS Simulations

The MPS implementation described in Section 3 of Rino et al. [3] is implemented with an exact propagator. The angular extent of the complex field spectral intensity can be measured directly. For reference, the incremental phase SDF is

$$\Phi_\phi(\kappa_y) = C_p \left\{ \begin{array}{c} {\kappa_y}^{-p_1},\ \kappa_y \leq \kappa_0 \\ ({\kappa_0}^{p_2-p_1}){\kappa_y}^{-p_2},\ \kappa_y > \kappa_0 \end{array} \right. . \tag{5}$$

An MPS operation multiplies the complex field at x_n by an incremental phase-screen contribution to generate

$$\psi_{n+\delta}(y) = \psi_n(y) \exp\{ik\phi(y)\}. \tag{6}$$

The MPS propagation step is implemented as follows:

$$\widehat{\psi}_{n+\delta}(\kappa_y) = \int \psi_{n+\delta}(y) \exp\{-i\kappa_y y\} \frac{d\kappa_y}{2\pi} \tag{7}$$

$$\begin{aligned} \psi_{n+1}(y) = \int \widehat{\psi}_{n+\delta}(\kappa_y) \left[\exp\{i \left(\sqrt{1-(\kappa_y/k)^2} - 1 \right) (k\rho_F)^2\} \right] \\ \times \exp\{i\kappa_y y\} d\kappa_y / (2\pi) , \end{aligned} \tag{8}$$

where $k = 2\pi f_c/c$, and $\rho_F = \sqrt{\Delta x/k}$ is the Fresnel scale. Narrow-angle propagation constrains the contributions as $\kappa_y \to k$. If the contributions are negligible, the factor in square brackets reduces to $\exp\{\pm i \left(\kappa_y \rho_F\right)^2 /2\}$.

The defining equations, (6), (7), and (8) are written as integrations of continuous functions. It is understood that for applications each integration is replaced by a Riemann sum over a finite range such that:

$$y(n\Delta y) = n\Delta y \text{ for } 0 \leq n \leq N-1 \tag{9}$$

$$\kappa_y(m) = m\Delta\kappa \text{ for } -N/2 \leq m \leq N/2-1 \tag{10}$$

$$\Delta\kappa = 2\pi/(N\Delta y) \tag{11}$$

with $dy \sim \Delta y$ and $d\kappa_y \sim \Delta\kappa$. A a minimum sampling interval $\Delta z > 200\lambda$ was found empirically. MPS propagation through a uniformly structured 50 km region followed by 200 km of free-propagation to an observation plane was used to generate realizations. With $v_{\text{eff}} = 152.6$ mps the realizations can be interpreted as a GNSS time series.

Phase screen realizations were generated for representative EPB structure with $p1 = 2.0$ and $p2 = 3.25$ and PPB structure with $p1 = 3.0$ and $p2 = 1.5$. In Rino et al. [3] turbulent strength was adjusted to produce extreme scintillation in the free-space propagation range, which is recovered perfectly with back propagation. To explore MPS saturation, the MPS extent was increased from 30 to 50 km followed by free propagation to 250 km. Figure 1 summarizes an EPB development with strong scintillation realized in the free-propagation

range. The upper frame displays the PSD evolution with measured $S4$ overlaid, red indicating MPS and blue indicating free-space. Spatial wave number has been converted to a direction angle $\theta = 2\pi\kappa_y/k$. In free space the PSD is invariant, whereby the initiating phase structure determines the range of propagation angles independent of evolving amplitude structure. The middle and lower frames show, respectively, intensity and phase at the 250 km observation range. Figure 2 shows the same simulation with C_P increased by 30 dB. Here strong focusing ($S4 > 1$) develops within the layer with the contributing range of propagation angles spanning $\pm 90^\circ$ with speckle-like ($S4 = 1$) saturation structure.

Phase-screen scintillation theory predicts constant $S4 \geq 1$ limits as the Fresnel scale increases indefinitely Carrano and Rino [4], whereas MPS limits exhibit a limiting exponential distribution with $S4 = 1$. Intensity PDFs are formally defined by fractional moments

$$M_m =< I^m > / < I >^m \ . \tag{12}$$

The critical moments are $m = 2$, 3, and 4. They define all the analytic intensity PDF models, often combined to define skew $K3 = (M_3 - 3M_2 + 2)/S4^{3/2}$ and kurtosis $K4 = (M_4 - 4M_3 + 6M_2 - 3)/S4^2$, where $S4 = \sqrt{M_2 - 1}$. For an exponential distribution $M_m = m!$. Figure 3 summarizes the development of the fractional moments for the moderate (upper frame) and extreme (lower frame) simulations. Each moment is normalized to exponential value to demonstrate convergence to exponentially distributed intensity scintillation with $S4 = 1$. The phase-screen theoretical limits apply strictly to phase screen realizations with a narrow range of propagation angles.

The peaks in the normalized fractional moments in the upper frame of Figure 3 are attributed to refractive changes induced by large-scale structure, which can vary significantly from realization to realization. $K4$ values greater than 3 are observed. We also find that in the moderate to strong focusing regime the $\alpha - \mu$ distribution, which is defined by $K3$ and $K4$, provides a good fit to the intensity PDFs. Similar behavior is observed with scintillation data. Figures 4, 5, and 6 shows the evolution of moderate and strong PPB structure. For this particular example PPB did not generate strong focusing. We note also that saturation is achieved with much smaller C_p values.

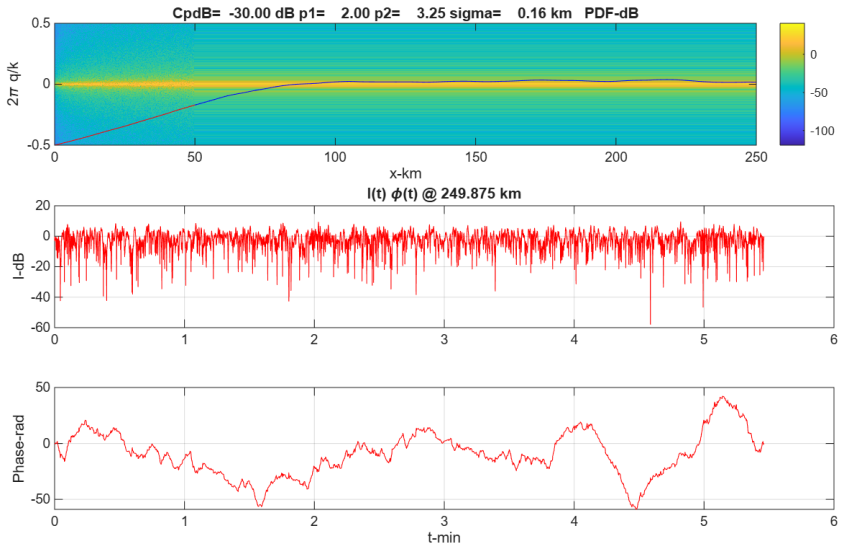


Figure 1: Top frame shows evolution of moderate EPB complex feld PSD versus radian propagation angle with $S4/2 + 0.5$ overlaid (0 to 1.5) red => MPS blue => free space. Middle and lower frames show intensity and phase versus time.

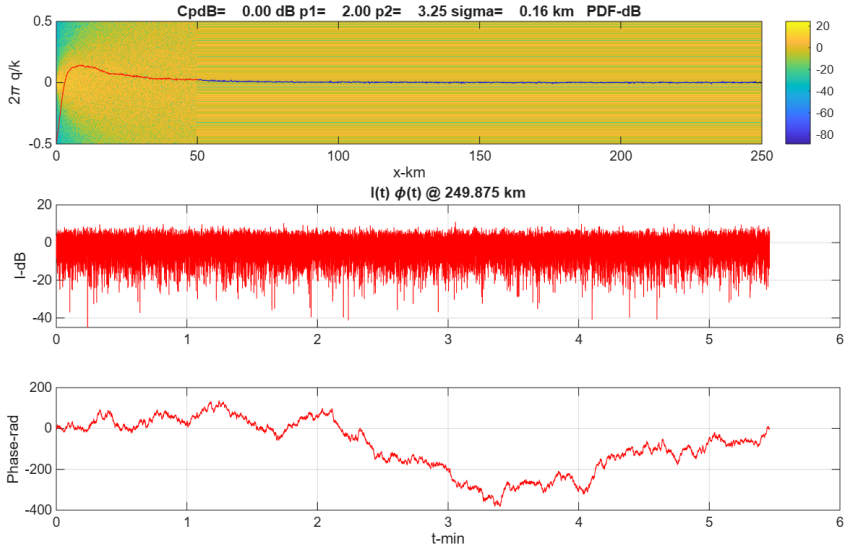


Figure 2: Evolution summary of strong EPB complex field. Same format as Figure 1

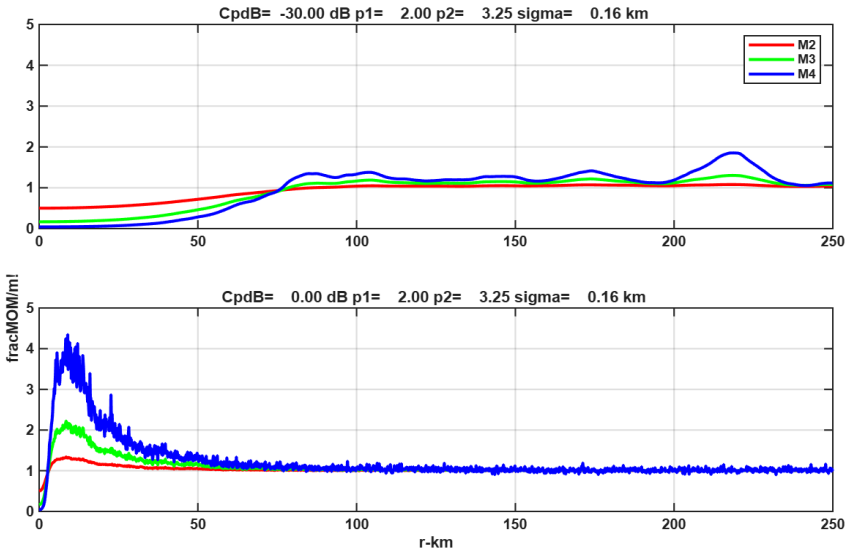


Figure 3: Moderate (upper frame) and strong (lower frame) evolution of fractional signal moments for EPB structure.

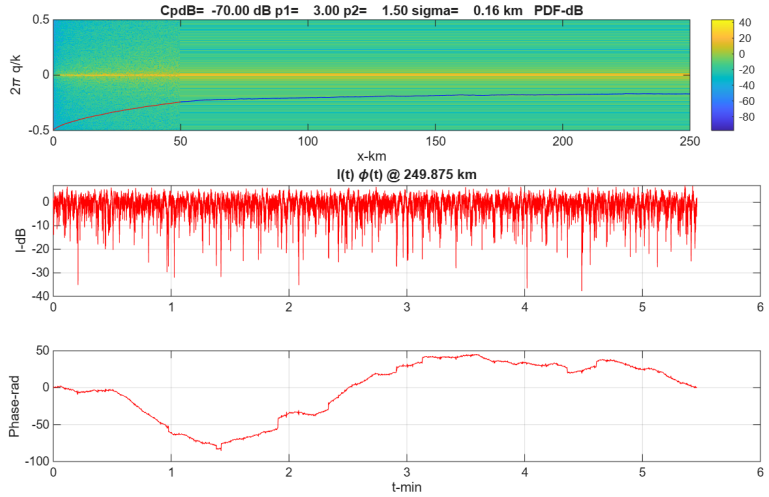


Figure 4: Top frame shows evolution of moderate PPB complex feld PSD versus radian propagation angle with $S4/2 + 0.5$ overlaid (0 to 1.5) red => MPS blue => free space. Middle and lower frames show intensity and phase versus time.

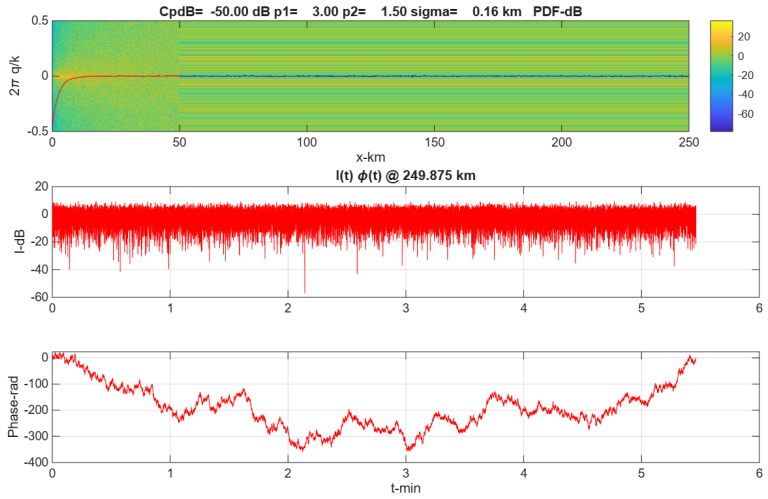


Figure 5: Evolution summary of strong PPB complex field. Same format as Figure 4

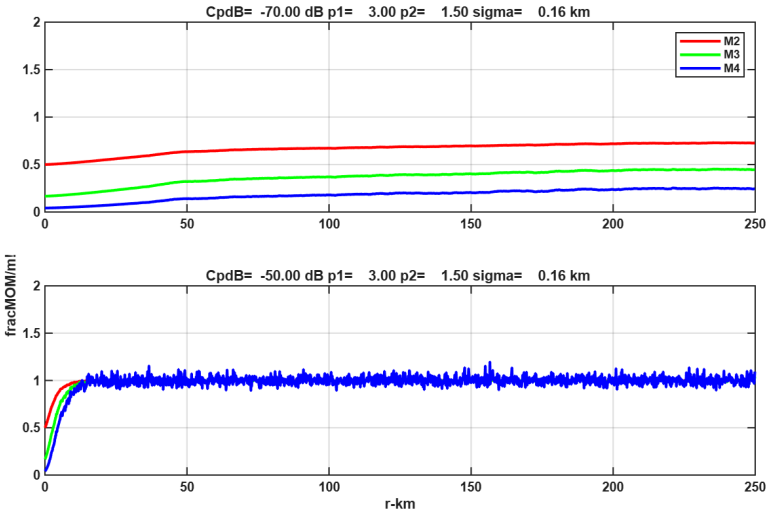


Figure 6: Moderate (upper frame) and strong (lower frame) evolution of fractional signal moments for PPB structure.

The universal strength parameter

$$U = C_P \begin{cases} \rho_F^{p_1-1} & \text{for } \mu_0 \leq 1 \\ \rho_F^{p_2-1} \mu_0^{p_1-p_2} & \text{for } \mu_0 \leq 1 \end{cases}, \tag{13}$$

where $\mu_0 = \kappa_0 \rho_F$, is a phase screen measure of scintillation intensity. As such it is formally restricted in both the the p_1 and p_2 ranges and narrow propagation angles. However, is shows that large $p_1$values can produce strong scintillation at smaller C_P values.

3 Back Propagation

Back propagation (BP) was used in Rino et al. [3] to validate irregularity parameter estimation (IPE) applied to reconstructed phase following BP. BP starts with the free-propagation hypothesis

$$\psi_{\rm BP}(y) = \int \widehat{\psi}(\kappa_y) \left[\exp\{-i \left(\sqrt{1 - (\kappa_y/k)^2} - 1 \right) (k\rho_F)^2 \} \right] \times \exp\{i\kappa_y y\} d\kappa_y / (2\pi) \,. \tag{14}$$

A starting distance equal to the estimated free-space propagation distance initiates a minimization operation. For simulated data the free-space propagation distance is known. If BP significantly reduces the intensity scintillation the extracted phase structure generally reproduces the initiating structure parameters with small errors. Figures 7 and 8 summarize BP/IP applied to EPB observation range complex fields similar to the simulations summarized in Figures 1 and 2. Figures 9 and 10 summarize BP/IP applied to the PPB observation range complex fields similar to the simulations summarized in Figures 3 and 4 . In all cases BP reduced the number of deep fades. For the moderate cases there is a significant reduction in $S4$ consistent with earlier findings. Because of uncorrected phase jumps there can be large absolute differences between the initiating and recovered phase. However, a *memory* of the large scale structure persists. In effect, differences is the spectral index at large scales is preserved. However, as the structure intensity increases resolving two-component structure is lost. EPB structure is misinterpreted as single power law with $p < 2$. PPB structure is misinterpreted as single power law with $p > 2$. Structure parameter estimates are validated by comparing the theoretical phase SDFs with the SDFs derived from the BP recovered phase and the theoretical SDFs with the estimated structure parameters. The BP distance that generates the minimum intensity variance if a true minimum is found is longer than the free propagation distance. If no minimum is found, the free propagation distance is use for BP. In all cases IPE provides a good fit to the measure SDF. This can be seen by comparing the green theoretical curves to the measured SDFs in the lower frames of Figures 7, 8, 9 and 10.

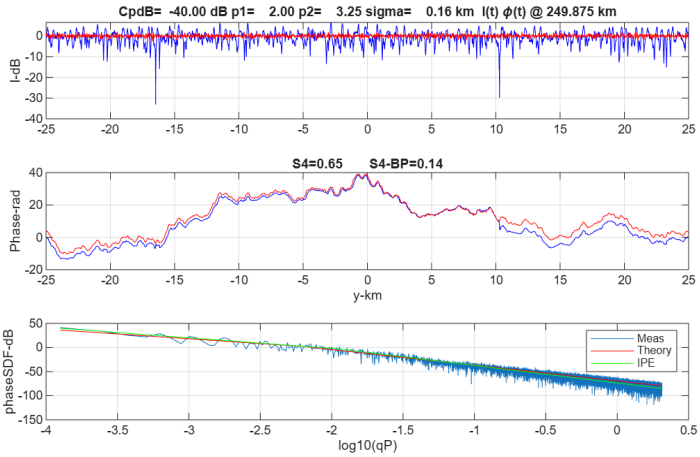


Figure 7: Upper frame shows observation range intensity (blue) and BP intensity (red). Middle frame shows phase (blue) and BP phase(red). Lower frame shows measured phase SDF(blue), theory (red), and IPE (green). EPB moderate.

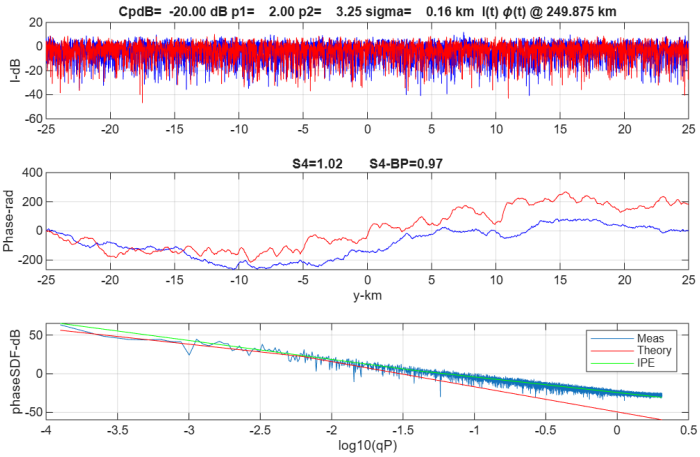


Figure 8: Upper frame shows observation range intensity (blue) and BP intensity (red). Middle frame shows phase (blue) and BP phase(red). Lower frame shows measured phase SDF(blue), theory (red), and IPE (green). EPB extreme.

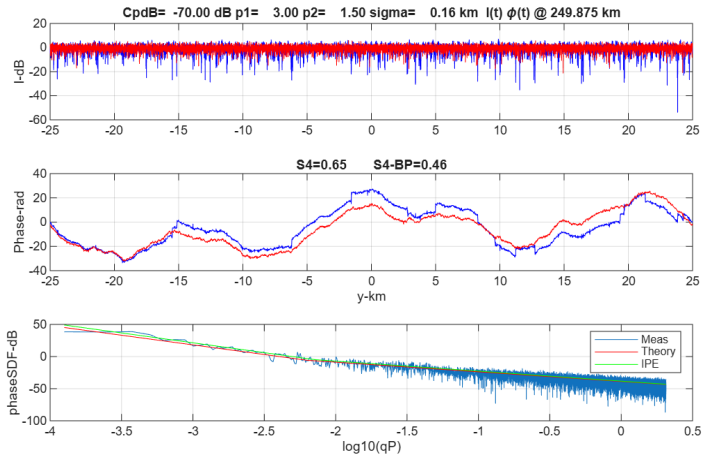


Figure 9: Upper frame shows observation range intensity (blue) and BP intensity (red). Middle frame shows phase (blue) and BP phase(red). Lower frame shows measured phase SDF(blue), theory (red), and IPE (green). PPB moderate.

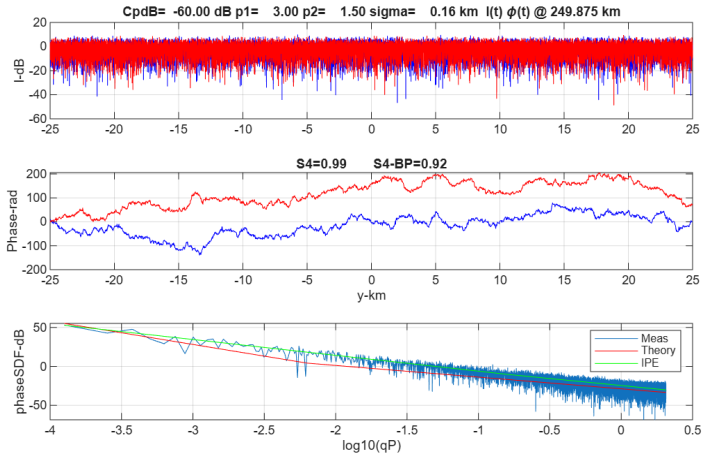


Figure 10: Upper frame shows observation range intensity (blue) and BP intensity (red). Middle frame shows phase (blue) and BP phase(red). Lower frame shows measured phase SDF(blue), theory (red), and IPE (green). PPB extreme.

4 Summary and Conclusions

Propagation in random media generally applies to propagation from a source to a receiver along a straight or gently curved path to accommodate occultations. In effect, refraction of the propagation path, as predicted by ray tracing, is excluded. Even within the constraints of a scalar propagation theory accommodating refraction is computationally demanding to an extreme. The problem is coupling between the media interaction terms in the wave equation, $X(x, y)$ or $X(\mathbf{r})\overline{\chi}$, and the propagation terms, ∇^2. A *sufficient* condition for decoupling is the narrow range of propagation angles constraint. However, the key finding in this paper is that for propagation in random medium this is not a *necessary* condition. This implies that if you want to explore *any* aspect of propagation in a random medium, MPS simulations are more accurate than theoretical results based on moment equations that use the parabolic approximation.

The examples used to demonstrate extreme simulations were two-dimensional idealizations with an extended region of homogeneous propagation disturbance followed by a prescribed free propagation distance. However, the results can be generalized to fully three-dimensional realizations. Configurations of random striations along parallel field lines have been explored . The simulations are readily generalized to configurations along curved field lines. Reducing the dimensionality of stochastic variation greatly simplifies computation, and it may be necessary for back propagation. In any case, guidelines from the simulations in this paper suggest that single-power-law estimates with $p_1 \sim p_2 < 2$ are EPB candidates. Structure estimates with $p_1 - p_2 > 1$ remain PPB candidates, particularly if $p_1 \geq 3$ indicating pronounced large scale structure.

References

[1] A. K. Sun, X. Pi, C. Rino, and J. Lee. Statistical uncertainty in the frequency dependence of the intensity scintillation index s4. *Radio Science*, 58, 2023. doi:org/10.1029/2023RS007659.

[2] Louis Fishman. Applications of directional wavefield decomposition, phase space, and path integral methods to seismic wave propagation and inversion. *Pure and Applied Geophysics*, 159:1637–1679, 2002.

[3] Charles Rino, Charles Carrano, Dmytro Vasylyev, Theodore Beach, Brian Breitsch, Yu Morton, and Keith Groves. Extreme scintillation structure diagnostics. *Journal of Atmospheric and Solar Terrestial Physics*, 282, 2026. https://doi.org/10.1016/j.jastp.2026.106805.

[4] C. Carrano and C. Rino. A theory of scintillation for two-component power law irregularity spectra: Overview and numerical results. *Radio Science*, 51:789–813, 2016. doi:10.1002/2015RS005903.